Zeng, R.; Hu, Y.; Zhang, F.; Huang, Y.; Wang, Z.; Li, S.; Han, E.:

Corrosion resistance of cerium-doped zinc calcium phosphate chemical conversion coatings on AZ31 magnesium alloy

In: Transactions of Nonferrous Metals Society of China (2017)
Elsevier / Allerton Press

DOI: 10.1016/S1003-6326(16)64102-X

Corrosion resistance of cerium-doped zinc calcium phosphate chemical conversion coatings on magnesium alloy AZ31

Rong-chang ZENG[1, 2], Yan HU[1, 2], Fen ZHANG[1, 2],Yuanding HUANG[4], Zhen-lin WANG[3], Shuo-qi LI[1, 2], En-hou HAN[5]

1. College of Materials Science and Engineering, Shandong University of Science and Technology, Qingdao 266590, China;
2. State Key Laboratory of Mining Disaster Prevention and Control Co-founded by Shandong Province and the Ministry of Science and Technology, Shandong University of Science and Technology, Qingdao 266590, China;
3. School of Materials Science and Engineering, Chongqing University of Technology, Chongqing 400054, China;
4. MagIC-Magnesium Innovation Center, Helmholtz-Zentrum Geesthacht, Zentrum für Material-und Küstenforschung GmbH, Geesthacht D-21502, Germany;
5. National Engineering Center for Corrosion Control, Institute of Metals Research, Chinese Academy of Science, Shenyang 110016, China

Abstract

Zinc calcium phosphate (Zn-Ca-P) coating and cerium-doped zinc calcium phosphate (Zn-Ca-Ce-P) coating were prepared on magnesium alloy AZ31. The chemical compositions, morphologies and corrosion resistance of the coatings were investigated through EDS, XPS, XRD, EPMA and SEM together with hydrogen volumetric and electrochemical tests. The results indicated that both coatings predominately

Foundation item: Project (51571134, 2014TDJH104, cstc2012jjA50034) supported by National Natural Science Foundation of China, the SDUST Research Fund, the Joint Innovative Centre for Safe and Effective Mining Technology and Equipment of Coal Resources, Shandong Province, and Natural Science Foundation of Chongqing.

Corresponding author: Rong-chang ZENG; Tel: +86-0532-80681226; E-mail address: rczeng@foxmail.com

contained crystalline hopeite ($Zn_3(PO_4)_2 \cdot 4H_2O$), $Mg_3(PO_4)_2$ and $Ca_3(PO_4)_2$, and traces of non-crystalline MgF_2 and CaF_2. The Zn-Ca-Ce-P coating was more compact than the Zn-Ca-P coating due to the formation of $CePO_4$, and displayed a better corrosion resistance than the Zn-Ca-P coating. Both coatings protected the AZ31 substrate only during an initial immersion period. The micro-galvanic corrosion between the coatings and their substrates led to an increase in HER with extending immersion time. Addition of Ce promoted the homogenous distribution of Ca and the formation of the hopeite. The Zn-Ca-Ce-P coating has the potential for the primer coating on magnesium alloys.

Keywords: magnesium alloy; cerium; calcium; chemical conversion coating; corrosion

1 Introduction

Magnesium alloys have become the preferred alternative structural materials in the aerospace and automobile industries due to their low density, high strength-to-weight ratio and recyclability [1, 2]. However, their applications are hindered, to a certain degree, because of their low corrosion resistance [3, 4]. Thus, considerable measures have been taken to improve the corrosion resistance of magnesium alloys. In addition to alloying [5], post processing and surface treatments including chemical conversion [6], anodic oxidation [7, 8], electroplating [9], electroless plating [10], thermal spraying [11], magnetron sputtering [12], organic coating [13], ion implantation [14] as well as laser processing [15] and their composite coating [16] have been used. In particular, chemical conversion coatings such as the chromium [17], phosphate [17], phosphate-potassium permanganate [18], rare earth [19-21], stannate [22], silane [23, 24] and phytic acid [25, 26] together with fluorozirconate [27] and layered double hydroxides (LDH) [28, 29]are regarded as the most effective approaches to protect magnesium alloys. Unfortunately, chromium conversion coatings are highly toxic and are carcinogenic [3]. Thus, environmentally friendly conversion coatings are required.

Currently, scientists are interested in rare earth and phosphate conversion coatings due to their environmentally friendly characteristics. Rare earth conversion coatings, formed by adding rare earth salts such as cerium, nitrate and lanthanum nitrate into chemical conversion baths, lead to a remarkable increase in the corrosion resistance of magnesium alloys [3, 30-32]. Moreover, the rare earth conversion film is utilized as the precursor for micro-arc oxidation (MAO) to obtain a cerium-containing coating. Additionally, it is found that the pre-treatment of the AZ91D alloy can effectively incorporate cerium oxides into the MAO coating and improve the performance of the MAO coating [33].

Phosphate conversion coatings are regarded as suitable alternatives to chromate conversion coatings because of their low toxicity and appropriate properties [34]. To date, there are six types of phosphate conversion coatings on magnesium alloys [35]: the Zn-P system [36-39], the Mn-P system [18, 40, 41], the barium phosphate (B-P) system [42], the molybdate phosphate (Mo–P) system [43], the Zn-Ca-P system [35, 44] and the cerium phosphate (Ce-P) system [45]. Usually, Zn-P coating contains two layers [37, 46, 47] with $AlPO_4$, MgF_2, $Mg_3(PO_4)_2$ and $MgZn_2(PO_4)_2$ [38]. The formation of the Zn-P coating is affected by the microstructure (i.e., intermetallic compounds) of the substrate alloys [37]. The Mn-P coating on AZ91D alloy is prepared at a temperature of 80 °C [40]. And the Mo–P coating formed on AZ31 magnesium alloys consists of mixed phases of $Mg(OH)_2$, MoO_2, MoO_3, and MgF_2 [43]. Our previous studies [48, 49] demonstrated that the introduction of Ca^{2+} ions into a zinc phosphate bath can promote the formation of a Zn-Ca-P coating and refine the microstructure of the coating, thus improving the corrosion resistance of the AZ31 alloy. Moreover, a crystalline Zn-Ca-P coating with a more fine-grained structure provides a superior corrosion resistance to that of the Zn-P coating on the AZ31 alloy. The formation and corrosion resistance of the Zn-Ca-P coating are significantly influenced by its microstructure as well as the chemical composition of the Mg-Al alloy [50]. A further exploration revealed that the optimum temperature of a phosphating bath is 55 °C for the Zn-Ca-P coating on a Mg−Li−Ca alloy [51]. However, the microstructure

of the Zn-Ca-P coating on magnesium alloys still needs further improvement. Additionally, its corrosion mechanism is not yet well understood.

This paper aims to modify the microstructure and improve the corrosion resisting property of the Zn-Ca-P conversion coating by doping with cerium and to gain insight into the formation and corrosion mechanism of the Zn-Ca-Ce-P coated alloy.

2 Experimental

2.1 Preparation of coatings

The experimental material was commercial rolled AZ31 alloy (nominal chemical compositions: 3 wt. % Al, 1 wt. % Zn, and Mg, Bal.), which was supplied by Beijing Guangling Jinghua Science & Technology, Co., Ltd. Samples with a dimension of 20 mm × 20 mm × 3 mm were ground with SiC emery paper up to 2000 grit to achieve a smooth surface. Prior to the preparation of coating, the samples were degreased in an alkaline solution, then in an acidic solution, and finally rinsed in distilled water and dried by warm air. The deposition of the Zn-Ca-P coating was carried out by immersing in a phosphating bath, which contained 10.0 g/L Na_2HPO_4, 4.0 g/L $NaNO_2$, 6.0 g/L $Zn(NO_3)_2$, 2.0 g/L $Ca(NO_3)_2$ and 2.0 g/L NaF. For the preparation of the Zn-Ca-Ce-P coating, 1.0 g/L $Ce(NO_3)_3$ was added to the solution mentioned above. The bath pH value was adjusted to 2.5 by adding phosphoric acid. All samples were immersed in the phosphating bath at 50 °C for 20 minutes.

2.2 Hydrogen evolution tests

The corrosion rate of the substrate and its coatings can be monitored by the hydrogen evolution volume. The evolved hydrogen volume was read per hour during an immersion period of 24 h in 3.5 wt. % NaCl solution at room temperature. The hydrogen evolution rate (HER) can be calculated by the equation

$$\mathrm{HER} = V_H / st \qquad (1)$$

where V_H is the hydrogen evolution volume (ml), s is the exposed area (cm^2) and t is the immersion time (h).

2.3 Surface analysis

The morphologies of the coatings before and after corrosion testing were observed using a scanning electron microscope (SEM, KYKY-2800B). The cross-sectional microstructures and energy-dispersive X-ray spectrum (EDS) were inspected by an electron probe micro-analyser (EPMA, JXA-8230). The composition of the coatings was identified by X-ray diffraction (XRD, D/Max 2500PC) and X-ray photoelectron spectroscopy (XPS).

3 Results

3.1 Surface morphologies

The surface morphologies of the Zn-Ca-Ce-P and Zn-Ca-P coatings are shown in Fig. 1. The Zn-Ca-Ce-P coating had a long, ridge-like crystalline structure (approximately 1-2 μm thick) and short, flake-shaped crystalline precipitates with particles embedded between the ridges (Fig. 1a). The Zn-Ca-Ce-P coating on the cross-sectional view (Fig. 1b) reveals that it contains a double-layer structure, an outer layer with a ridge-like crystalline microstructure and an inner layer with a compact microstructure with micro cracks. However, no through cracks were found on the whole Zn-Ca-Ce-P coating (Fig. 1b). It is worth noting that the Zn-Ca-P coating resembles a flower-like morphology with a refined microstructure and cracks, which were obviously observed among the flower-like structures (Fig. 1c). This result was in agreement with our previous study [50]. However, the Zn-Ca-P coating has considerable through cracks (Fig. 1d), which led to a reduction in the compactness of the Zn-Ca-P coating and its adhesion to the substrate.

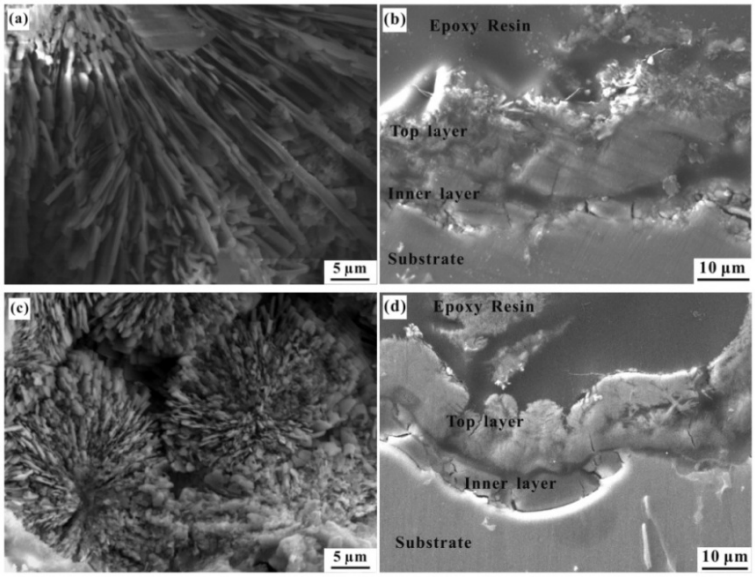

Fig. 1 SEM micrograph and cross-sectional views of (a), (b) the Zn-Ca-Ce-P coating; (c), (d) the Zn-Ca-P coating.

3.2 Chemical compositions and constitutions

Fig. 2 designates the spectrums and detected sites of the coatings. Both coatings are composed of the elements O, Zn, P, Mg, F, Al and Ca (Table 1). The existence of C is ascribed to the sprayed carbon on the surface of the samples prior to the EPMA examination. The Zn-Ca-Ce-P coating exhibits a higher Mg content. The high content of F in the non-crystalline areas (Spectra 1 and 3 in Fig. 2a and Spectrum 3 in Fig. 2b) implies the possible presence of MgF_2, CeF_3 and CaF_2, whereas no F was detected in the crystallized areas (Spectrum 2 in Fig. 2a and Spectrum 1 in Fig. 2b). This scenario demonstrates that MgF_2, CeF_3 and CaF_2 are heterogeneously distributed in these two coatings. The presence of Zn and Ca is derived from the species of the solutions. Our previous investigation [49] also indicated that $CaHPO_4$ and $Ca_3(PO_4)_2$ are located in the outer layer of the Zn-Ca-P coating. The contents of Zn and P in the Zn-Ca-Ce-P coating are higher than that in the Zn-Ca-P coating (Table 1). In comparison with the Zn-Ca-P coating, obviously, the higher concentration of Zn may be attributed to its higher crystallinity of the Zn-Ca-Ce-P coating. This result suggests that a high amount of hopeite covered the Zn-Ca-Ce-P coating.

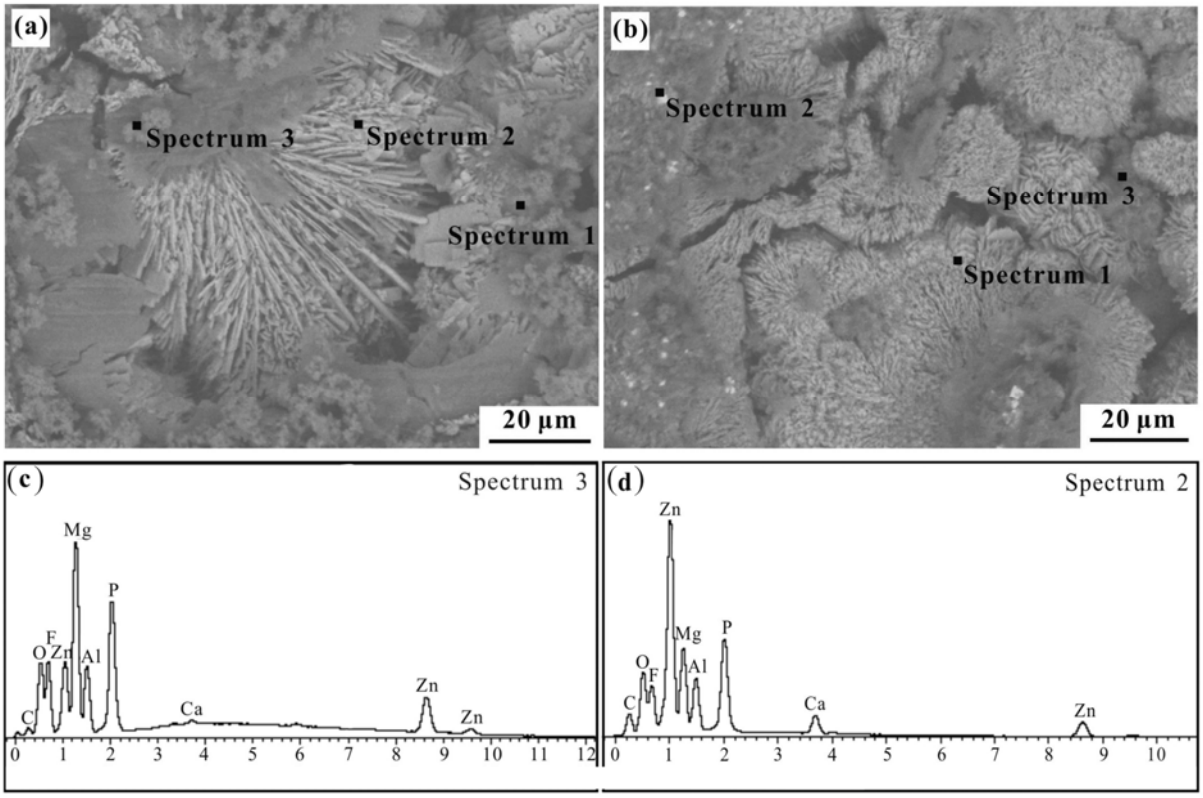

Fig. 2 SEM images and corresponding EDS mappings of (a) the Zn-Ca-Ce-P and (b) the Zn-Ca-P coatings.

Table 1 Chemical compositions of the coatings in different positions (wt. %).

Coatings	Spectrums	Elements							
		C	O	Mg	F	Al	P	Zn	Ca
Zn-Ca-Ce-P	1	6.40	39.13	9.59	4.75	3.75	13.59	22.39	0.41
	2	10.61	31.65	7.03	-	1.66	18.42	30.41	0.21
	3	9.33	17.21	17.14	19.73	5.80	10.66	19.72	0.41
Zn-Ca-P	1	25.36	36.83	6.18	-	0.59	16.02	14.76	0.26
	2	5.14	54.81	6.20	-	7.63	13.71	12.04	0.48
	3	21.87	22.52	8 .67	20.16	5.03	8.87	10.65	2.23

The elemental mappings from a cross-sectional perspective (Fig. 3) show that the contents of Mg, P and O in the interior layer are significantly higher than in the exterior layer, but their concentration in the exterior layer of the Zn-Ca-Ce-P coating is lower than that of the Zn-Ca-P coating. It can be concluded that

$Mg_3(PO_4)_2$ is located in the inner layer of coating. This result is consistent with our previous investigation [49]. It is worth noting that the content of Zn in the exterior layer of the coatings is considerably higher than that in the interior layer, indicating that a high amount of hopeite deposited on the surface. The distribution of Ca is more homogeneous in the Zn-Ca-Ce-P coating than in the Zn-Ca-P coating (Fig. 3). The element Ce was not detected by EDS due to its lower content. This novel finding demonstrates that the introduction of Ce^{3+} ions promotes the homogeneity of the Ca distribution. Further investigations by XRD confirm this finding, too.

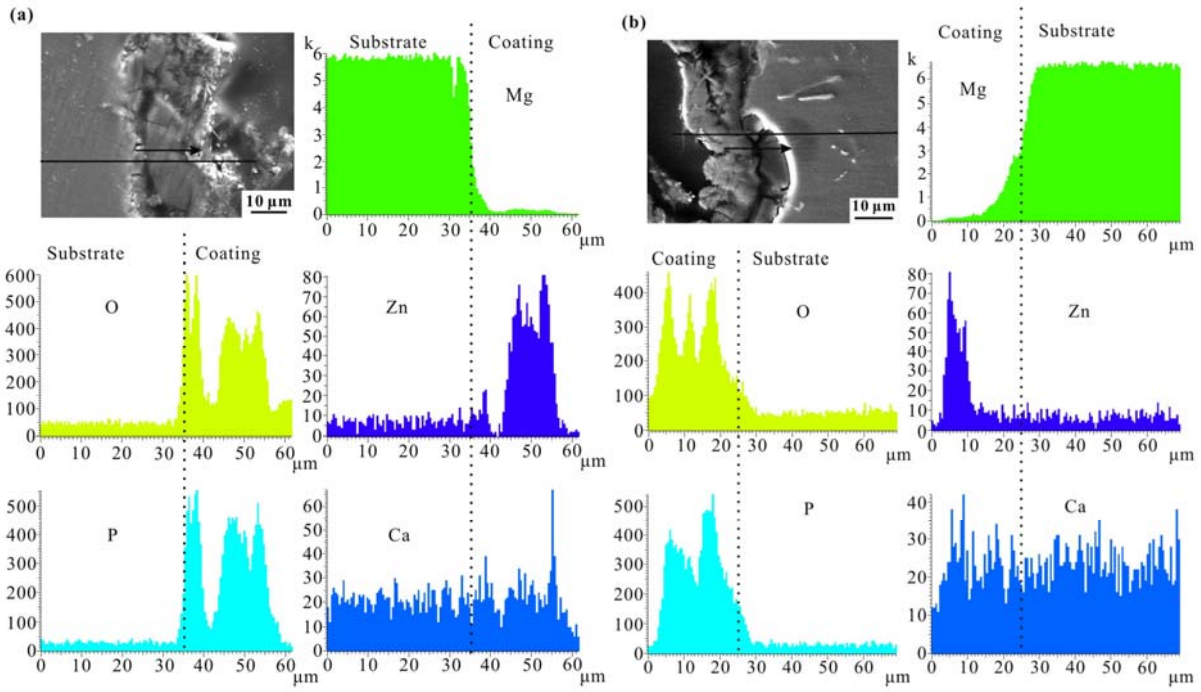

Fig. 3 Linear scanning mapping of the cross-sectional coatings: (a) the Zn-Ca-Ce-P and (b) the Zn-Ca-P coatings.

The XRD patterns for both coatings are quite different from each other (Fig. 4). The peak for the α-Mg phase designates the microstructure of the AZ31 substrate. The diffraction peaks of tetra-hydrated zinc phosphate ($Zn_3(PO_4)_2 \cdot 4H_2O$) manifest a higher intensity in the Zn-Ca-Ce-P coating than in the Zn-Ca-P coating. The weak diffraction peaks of $Mg_3(PO_4)_2$, $CePO_4$ and $Ca_3(PO_4)_2$ were detected in the Zn-Ca-Ce-P coating, that proved the existence of traces of $Mg_3(PO_4)_2$, $CePO_4$ and $Ca_3(PO_4)_2$, which became the nuclei of the coating. The peak for ZnO was found in the Zn-Ca-P coating [52]. The ZnO originated from the

dehydration of $Zn(OH)_2$. MgF_2, CeF_3 and CaF_2 were not identified by XRD due to their noncrystalline structures.

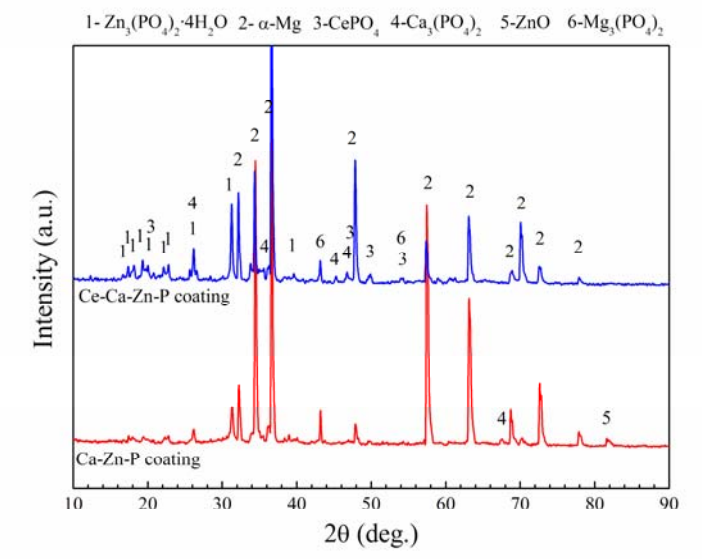

Fig. 4 XRD patterns of both coatings formed on the AZ31 alloy.

The compositions of the two coatings were probed by XPS to prove the existence and ascertain the form of cerium salts. The XPS spectra of the two coatings are depicted in Fig. 5. Fig. 5a shows that the Zn-Ca-Ce-P coating mainly consists of Mg, Zn, P, O, F, Ca and Ce, while Fig. 5b indicates that the Zn-Ca-P coating includes Mg, Zn, P, O, F and Ca. Meanwhile, the presence of C may be due to adventitious hydrocarbons from the environment.

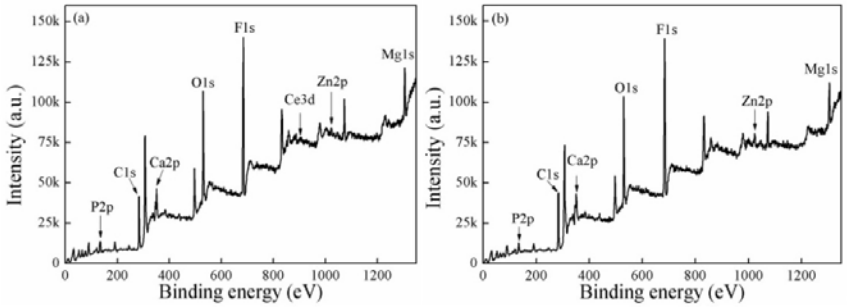

Fig. 5 XPS survey of two coatings: (a) the Zn-Ca-Ce-P coating and (b) the Zn-Ca-P coating.

Fig. 6 shows the high-resolution XPS spectra of the Zn, P, Ce and O elements on the Zn-Ca-Ce-P coating. The high-resolution spectra of Zn 2p (Fig. 6a) was divided into two peaks, which correspond to $Zn_3(PO_4)_2 \cdot 4H_2O$ and ZnO [49]. The P 2p peak correspond to $CePO_4$, $Zn_3(PO_4)_2 \cdot 4H_2O$, $Ca_3(PO_4)_2$ and

$CaHPO_4$ (Fig. 6b). The Ce 3d peaks reveal the presence of $CePO_4$ (Fig. 6c). The high-resolution spectrum of O 1s also confirms this result (Fig. 6d). According to results of the XPS spectra [3, 45, 49, 53], the peak positions and corresponding compounds were listed in Table 2.

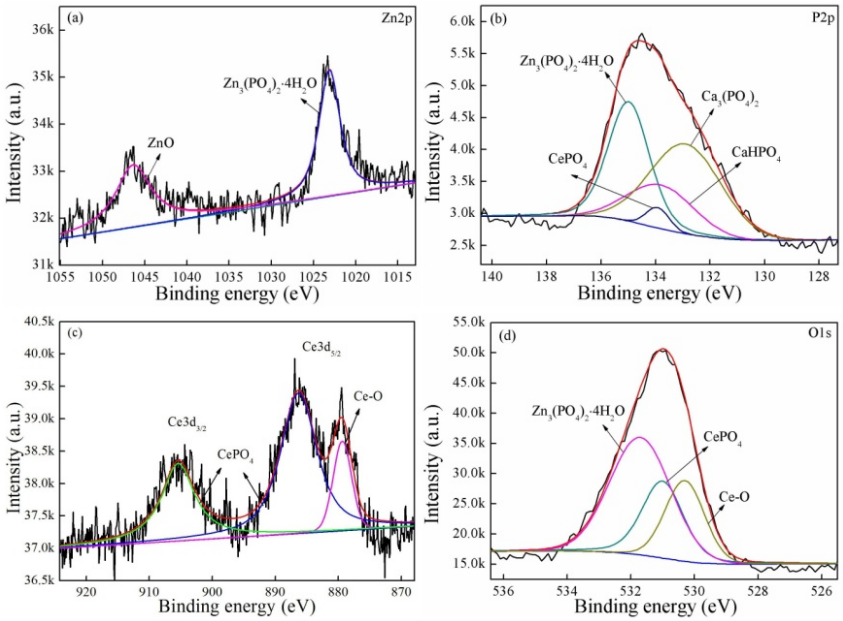

Fig. 6 High-resolution XPS spectra of the Zn-Ca-Ce-P coating: (a) Zn 2p, (b) P 2p, (c) Ce 3d, (d) O 1s.

Table 2 Peaks and corresponding compounds in high resolution XPS spectra.

Compounds	$Zn_3(PO_4)_2·4H_2O$	ZnO	$CePO_4$	Ce-O	$Ca_3(PO_4)_2$	$CaHPO_4$
Peaks (eV)	531.2	530.0	531.0	880.9	532.1	347.8
	1021.2	1044.7	133.3	882.2	346.9	

As with the Zn-Ca-P coating, the high-resolution spectra of Zn, P, Ca and O in the Zn-Ca-P coating are depicted in Fig. 7. Apparently, the spectrum of Zn 2p shown in Fig. 7a is consistent with that shown in Fig. 6a, proving the existence of $Zn_3(PO_4)_2·4H_2O$ and ZnO. The P 2p peak correspond to $Zn_3(PO_4)_2·4H_2O$, $Ca_3(PO_4)_2$ and $CaHPO_4$ (Fig. 7b). The high-resolution spectrum of Ca 2p can be decomposed into two peaks assigned to Ca $2p_{3/2}$ and Ca $2p_{1/2}$ peaks (Fig. 7c), and the Ca $2p_{1/2}$ peak is the satellite peak. The Ca $2p_{3/2}$ peak was assigned to CaF_2, $Ca_3(PO_4)_2$ and $CaHPO_4$. The O 1s peak shown in Fig. 7d is in good agreement with the Zn, P and Ca peaks. The results not only agree with the EDS and XRD results but also

further identify the presence of $CePO_4$ in Zn-Ca-Ce-P coating.

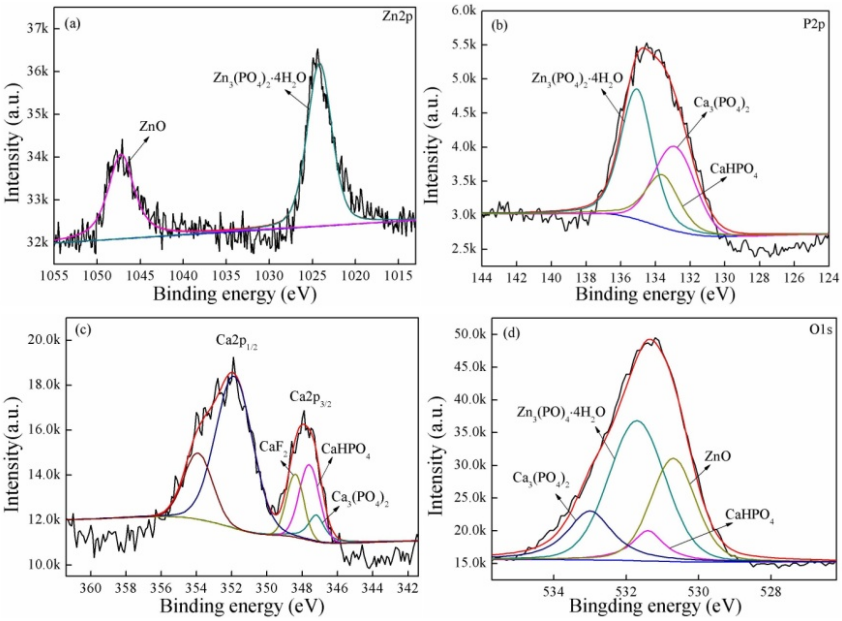

Fig. 7 High-resolution XPS spectra of the Zn-Ca-P coating: (a) Zn 2p, (b) P 2p, (c) Ca 2p, (d) O 1s.

4 Discussion

4.1 Formation mechanism of the Zn-Ca-Ce-P coating

The formation of the Zn-Ca-Ce-P coating may be different from the Zn-Ca-P coating that we previously studied [50] because of the introduction of $Ce(NO_3)_3$. Once magnesium alloys are immersed in an acidic phosphating bath, the α-Mg phase adjacent to the intermetallic compounds such as AlMn particles [49, 50] preferentially corroded according to the following electrochemical reactions (Fig. 8a):

$$Mg \rightarrow Mg^{2+} + 2e^{-} \quad (2)$$

$$2H_2O + 2e^{-} \rightarrow 2OH^{-} + H_2\uparrow \quad (3)$$

Ce^{3+} ions were oxidized to Ce^{4+} in the weakly acidic solution [54], leading to the formation of $Ce(OH)_4$ precipitates (Reactions (4) and (5)). Therefore, a $CePO_4$ precipitate (Fig. 8b) is preferentially formed because its solubility product constant (2.0×10^{-48}) is much lower than that of the $Ca_3(PO_4)_2$ compound (2.0×10^{-29}). The following reactions occurred successively in the acidic phosphating bath [53,

54].

$$4Ce^{3+} + O_2 + 2H_2O \rightarrow 4Ce^{4+} + 4OH^- \quad (4)$$

$$Ce^{4+} + 4OH^- \rightarrow Ce(OH)_4 \quad (5)$$

$$2Ce(OH)_4 + H_2 \rightarrow 2Ce(OH)_3 + 2H_2O \quad (6)$$

$$Ce(OH)_3 + 3H^+ + PO_4^{3-} \rightarrow CePO_4 + 3H_2O \quad (7)$$

The stability of $CePO_4$ is higher than that of $Ce(OH)_3$, especially in acid solution. The formation of $CePO_4$ (Fig. 6c) promoted the compactness of the Zn-Ca-Ce-P coating by reducing the amount of water trapped in the crystal [53].

At the same time, magnesium phosphate (Fig. 8c), calcium phosphate (Fig. 8d) and tetra-hydrated zinc phosphate (Fig. 8e) formed on the surface of the alloy [48-50]:

$$3Mg + 2H^+ + 2H_2PO_4^- \rightarrow Mg_3(PO_4)_2 + 3H_2\uparrow \quad (8)$$

$$Ca^{2+} + HPO_4^{2-} \rightarrow CaHPO_4 \quad (9)$$

$$3CaHPO_4 \rightarrow Ca_3(PO_4)_2 + H_3PO_4 \quad (10)$$

$$3Zn^{2+} + 2H_2PO_4^- + 2H^+ + 4H_2O + 6e^- \rightarrow Zn_3(PO_4)_2 \cdot 4H_2O + 3H_2\uparrow \quad (11)$$

$Zn_3(PO_4)_2 \cdot 4H_2O$ is the main component of the Zn-Ca-P coating [49]. Once the hopeite ($Zn_3(PO_4)_2 \cdot 4H_2O$) initially formed, Reaction (11) would not be interrupted until the film covered the whole surface (Fig. 8f).

Our previous work has proved that traces of MgF_2 and MgO may form as reaction (13) - (14) [52]. Meanwhile, CaF_2 and CeF_3 also formed:

$$Mg + 2H_2O \rightarrow Mg(OH)_2 + H_2\uparrow \quad (12)$$

$$Mg(OH)_2 + 2F^- + 2H^+ \rightarrow MgF_2 + 2H_2O \quad (13)$$

$$Mg(OH)_2 \rightarrow MgO + H_2O \quad (14)$$

$$Ce^{3+} + 3F^- \rightarrow CeF_3 \quad (15)$$

$$Ca^{2+} + 2F^{-} \rightarrow CaF_2 \quad (16)$$

Additionally, during the phosphating process, Zn^{2+} could obtain the electrons coming from the dissolution of magnesium and might therefore become single zinc and deposit on the surface [36, 48, 52]:

$$Zn^{2+} + 2e^{-} \rightarrow Zn \quad (17)$$

Nevertheless, Zn could not stay in the aggressive environment for a long time. It transformed into ZnO via the following reactions [52] :

$$Zn + 2H_2O \rightarrow Zn(OH)_2 + H_2\uparrow \quad (18)$$

$$Zn(OH)_2 \rightarrow ZnO + H_2O \quad (19)$$

Consequently, $Zn_3(PO_4)_2 \cdot 4H_2O$ and ZnO were detected by XRD in the Zn-Ca-P coating.

According to above discussion, the formation process of the Zn-Ca-Ce-P coating followed six steps: (1) the dissolution of the α-Mg matrix around the AlMn phase and release of hydrogen (Fig. 8a), (2) the nuclei of cerium phosphate formed initially and uniformly in solution (Fig. 8b), (3) the nuclei formation of magnesium phosphate (Fig. 8c), (4) calcium phosphate formed, and precipitated on surface of alloy with cerium phosphate, promoting the uniform formation of the dispersive nuclei of calcium phosphate (Fig. 8d), (5) the formation of zinc phosphate precipitates (Fig. 8e), (6) the coalescence of zinc phosphate precipitates mixed with calcium phosphate and cerium phosphate, and the formation of a crystalline zinc phosphate coating (Fig. 8f).

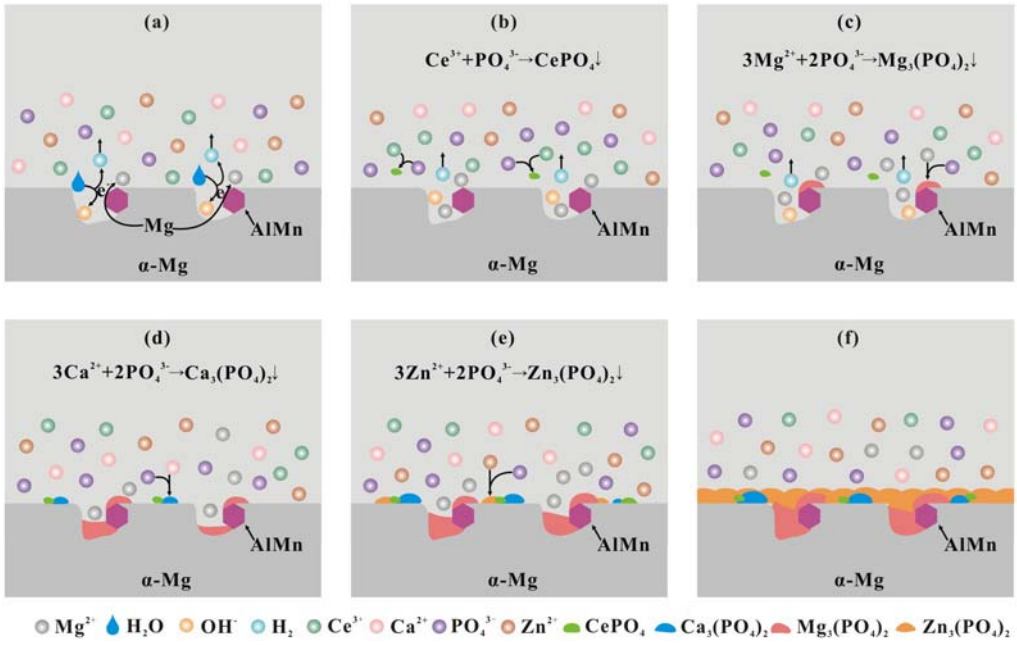

Fig. 8 Schematic diagrams for the formation of the Zn-Ca-Ce-P coating: (a) the dissolution of α-Mg matrix neighbouring the AlMn-phase and hydrogen release, (b) the formation of a nucleus of cerium phosphate, (c) nuclei formation of magnesium phosphate, (d) the formation of calcium phosphate, (e) the formation of a zinc phosphate nucleus and (f) the coalescence of the zinc phosphate nuclei and the formation of a crystalline zinc phosphate coating.

4.2 Corrosion mechanism of the Zn-Ca-Ce-P coated alloy

Based on the corrosion resistance derived from the hydrogen evolution (Fig. 9), the HERs of both coatings continuously increased with increasing immersion time, whereas the HER of the substrate did not rise until an immersion time of 6 h and descended successively and slowly. Fig. 9 shows that the corrosion processes of the coatings and substrate followed three stages: (I) both of the coatings had a lower corrosion rate than the substrate in an immersion time of 11 h; (II) the Zn-Ca-P coating had the highest corrosion rate, while the Zn-Ca-Ce-P coating had the lowest; and (III) the corrosion rates of both coatings were higher than that of the substrate after immersion for 17 h.

At stage I, both of the coatings had a lower corrosion rate than the substrate because of the protection

from the phosphate coating. A similar observation was also reported in our previous study [49] and by Li [31]. The rapid increase in the HER of the substrate during the initial stage is attributed to the dissolution of magnesium. However, at stages II and III, after the formation and thickening of the $Mg(OH)_2$ precipitate, which inhibited the attack from Cl^- ions, the HER of the substrate subsequently exhibited a slow decrease. In these stages, the HERs of the Zn-Ca-Ce-P and the Zn-Ca-P coatings surpassed that of their substrates, which were associated with the existence of coating defects such as voids and micro-cracks (Figs. 1b and 1d).

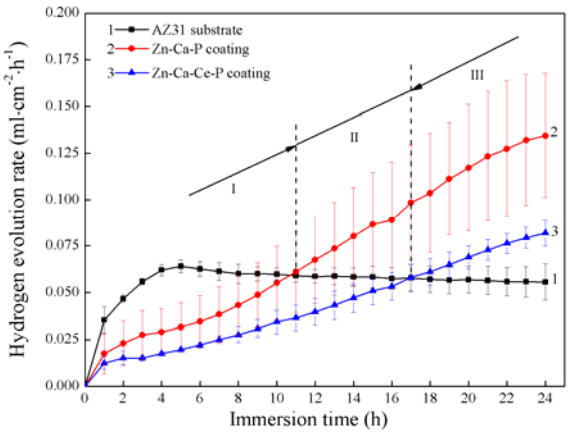

Fig. 9 Hydrogen evolution rates of the substrate and its coatings in 3.5 wt. % NaCl solution.

Fig. 10 displays the polarization curves for the AZ31 substrate and coated samples. The open corrosion potential (OCP), E_{corr} of the Zn-Ca-Ce-P and the Zn-Ca-P coatings were higher and the corrosion current density, I_{corr} were lower than that of the AZ31 alloy (Table 3). Especially, the I_{corr} of the Zn-Ca-Ce-P coating decreased by almost of one order of magnitude. This result was in pronounced accordance with the HER, indicating the Zn-Ca-Ce-P coating and the Zn-Ca-P coatings protected the alloy in initial immersion stage effectively.

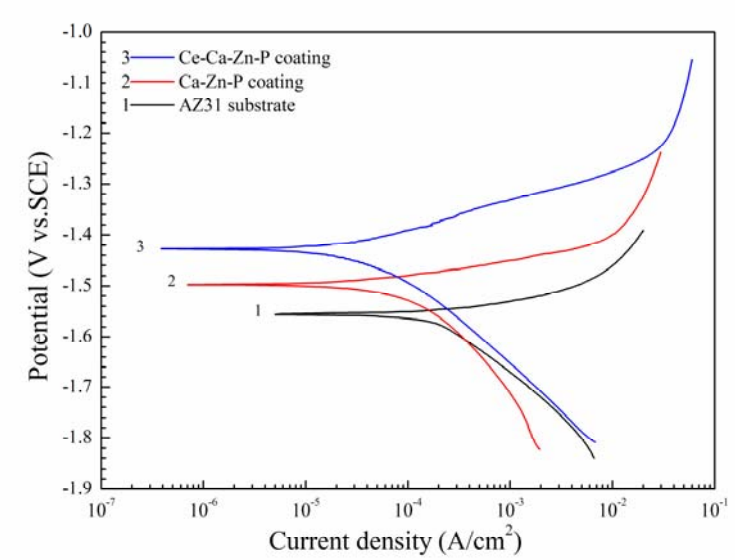

Fig. 10 Polarization curves for AZ31 and its coatings in 3.5 wt. % NaCl solution.

Table 3 Electrochemical parameters obtained from polarisation curves in 3.5 wt. % NaCl solution.

Samples	E_{corr} (V vs.SCE)	I_{corr} (A/cm^2)
AZ31 alloy	-1.55	2.04×10^{-4}
Zn-Ca-P coating	-1.49	1.12×10^{-4}
Zn-Ca-Ce-P coating	-1.43	4.50×10^{-5}

The localised exfoliation or detachment of the coatings (marked by an arrow in Fig. 11) could occur [46] and the substrate exposed to the solution. The Zn-Ca-Ce-P coating had less cracks than the Zn-Ca-P coating, and the exposed area of the substrate in the Zn-Ca-Ce-P coating were smaller (Fig. 11a) than those in the Zn-Ca-P coating (Fig. 11b). The Zn-Ca-Ce-P coating thus had a lower corrosion rate than the Zn-Ca-P coating.

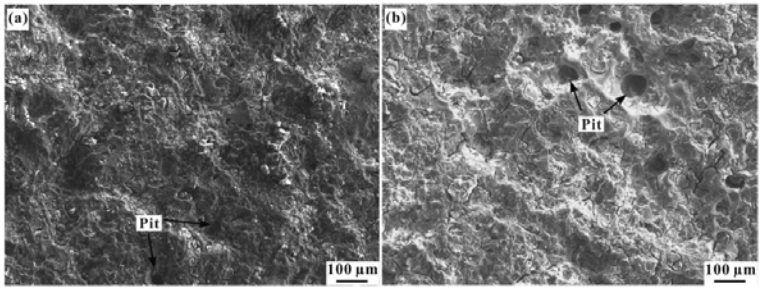

Fig. 11 SEM micrograph of the coatings after immersed for 24 h in 3.5 wt. % NaCl solution: (a) the

Zn-Ca-Ce-P coating, (b) the Zn-Ca-P coating.

The schematic diagram in Fig. 12 illustrates the corrosion mechanism of the Zn-Ca-Ce-P-coated alloy. After immersed in 3.5 wt. % NaCl solution, the corrosion process could be divided into three stages. In stage I, water rapidly diffused into the coating, and then the defects and micro-cracks inside the coating could provide a path for the penetration of water and Cl^- ions into the substrate (Fig. 12a). In stage II, the secondary phase/substrate interface was exposed to the solution. AlMn phase, having a higher corrosion potential than the α-Mg [55], acted as the micro cathode; whereas the Mg substrate acted as the micro anode. Micro-galvanic corrosion thus occurred, resulting in the formation of $Mg(OH)_2$ with a prolonged period of immersion (Fig. 12b). In stage III, the formation of $Mg(OH)_2$ sealed the voids and cracks of the coatings with extended immersion time. Unfortunately, corrosion still occurred in the sealed cracks and some of the coating peeled off due to the continuous generation of H_2 underneath the coating. More substrate was exposed to the solution and accelerated its corrosion rate (Fig. 12c). In view of the HERs of the coated alloys, the corrosion initiation of the Zn-Ca-Ce-P coated alloy was significantly delayed relative to the Zn-Ca-P coated alloy. This consequence implies that the chemical conversion coating could hardly protect the substrate from the corrosion for a long immersion time.

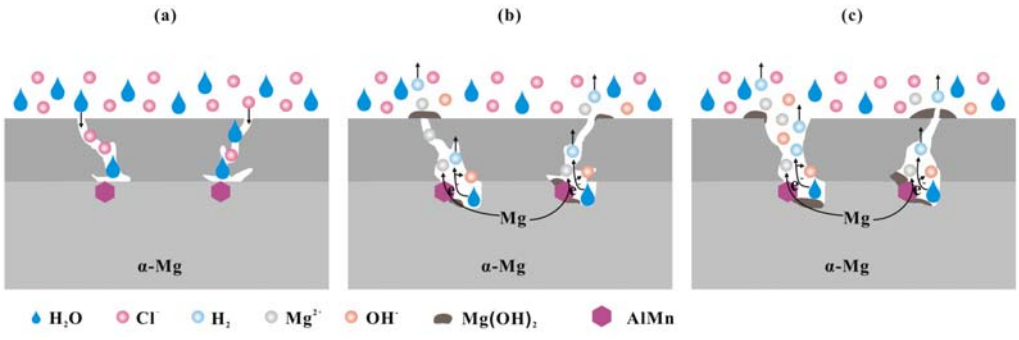

Fig. 12 Corrosion mechanism of the Zn-Ca-Ce-P coated AZ31 magnesium alloy.

5 Conclusions

The Zn-Ca-Ce-P and Zn-Ca-P coatings have been successfully fabricated on the AZ31 alloy. It is

concluded as following:

1) The Zn-Ca-Ce-P coating displayed a more compact double-structure with a ridge-like inner layer and a flake-like outer layer, while the Zn-Ca-P coating had a flower-like morphology with a considerable number of cracks and defects. And both coatings contained traces of noncrystalline products. The Zn-Ca-P coating was predominantly consisted of $Zn_3(PO_4)_2 \cdot 4H_2O$, $Mg_3(PO_4)_2$, $Ca_3(PO_4)_2$ and small amounts of MgF_2, CaF_2 and Zn/ZnO, while the Zn-Ca-Ce-P coating contained traces of $CePO_4$ and CeF_3 besides above compounds.

2) The introduction of Ce promoted the homogeneous distribution of Ca, the nuclei formation of hopeite, the compactness of the Zn-Ca-Ce-P coating, and thus resulting in a better corrosion resistance than the Zn-Ca-P coating. Both Zn-Ca-Ce-P and Zn-Ca-P coatings improved the corrosion resistance of the AZ31 substrate only over a limited immersion period.

3) The continuous decrease in the corrosion resistance of the coatings was attributed to the presence of micro cracks and through-voids inside the coatings. Micro-galvanic corrosion occurred between the secondary phases and the magnesium substrate, leading to an enlargement in the exposed area of the substrate, and thus an increase in HER over immersion time.

References

[1] ZENG Rong-chang, KE Wei, XU Yong-bo, HAN En-hou, ZHU Z Y. Recent development and application of magnesium alloys [J]. Acta Metallurgica Sinica, 2001, 37: 673-685. (in Chinese)

[2] SONG Guang-ling. Recent progress in corrosion and protection of magnesium alloys [J]. Advanced Engineering Materials, 2005, 7: 563-586.

[3] WANG Xi-mei, ZHU Li-qun, HE Xiang, SUN Feng-lou. Effect of cerium additive on aluminum-based chemical conversion coating on AZ91D magnesium alloy [J]. Applied Surface Science, 2013, 280: 467-473.

[4] SONG Guang-ling. Corrosion and protection of magnesium alloys [M]. 2nd ed. Beijing: Chemistry Industry Press, 2006. (in Chinese)

[5] ZENG Rong-Chang, SUN Lu, ZHENG Yu-Feng, CUI Hong-Zhi, HAN En-Hou. Corrosion and characterisation of dual phase Mg–Li–Ca alloy in Hank's solution: The influence of microstructural features [J]. Corrosion Science, 2014, 79: 69-82.

[6] HAN En Hou, ZHOU Wan Qiu, SHAN Da Yong, KE Wei, Corrosion and protection of magnesium alloy AZ31D by a new conversion coating [C]//Y. Kojima, T. Aizawa, K. Higashi and S. Kamados. Materials Science Forum. Trans Tech Publ, 2003: 879-882.

[7] CHEN Jun, ZENG Rong-Chang, HUANG Wei-Jiu, ZHENG Zi-Qing, WANG Zhen-Lin, WANG Jun. Characterization and wear resistance of macro-arc oxidation coating on magnesium alloy AZ91 in simulated body fluids [J]. Transactions of Nonferrous Metals Society of China, 2008, 18: s361-s364.

[8] ZHANG RF, ZHANG SF. Formation of micro-arc oxidation coatings on AZ91HP magnesium alloys [J]. Corrosion Science, 2009, 51: 2820-2825.

[9] WU Chao-yun, ZHANG Jin. Corrosion protection of Mg alloys by cathodic electrodeposition coating pretreated with silane [J]. Journal of coatings technology and research, 2010, 7: 727-735.

[10] LIU Zhen-min, GAO Wei. Electroless nickel plating on AZ91 Mg alloy substrate [J]. Surface and Coatings Technology, 2006, 200: 5087-5093.

[11] MAJUMDAR J D, BHATTACHARYYA U, BISWAS A, MANNA I. Studies on thermal oxidation of Mg-alloy (AZ91) for improving corrosion and wear resistance [J]. Surface and Coatings Technology, 2008, 202: 3638-3642.

[12] ZENG Rong-Chang, JIANG Ke, LI Shuo-Qi, ZHANG Fen, CUI Hong-Zhi, HAN En-Hou. Mechanical and corrosion properties of Al/Ti film on magnesium alloy AZ31B [J]. Frontiers of Materials Science, 2015, 9: 66-76.

[13] Ng W F, WONG M H, CHENG F T. Stearic acid coating on magnesium for enhancing corrosion resistance in Hanks' solution [J]. Surface and Coatings Technology, 2010, 204: 1823-1830.

[14] LIU Cheng-long, XIN Yun-chang, TIAN Xiu-bo, CHU P K. Corrosion behavior of AZ91 magnesium alloy treated by plasma immersion ion implantation and deposition in artificial physiological fluids [J]. Thin Solid Films, 2007, 516: 422-427.

[15] WANG Jing-feng, QIN Bin, WU Xia, PAN Fu-sheng, TANG Ai-tao. Current status and development of research on anti-corrosion technology for magnesium alloys [J]. Surface Technology, 2008, 37: 71-74.

[16] ZENG Rong-Chang, QI Wei-Chen, SONG Ying-Wei, HE Qin-Kun, CUI Hong-Zhi, HAN En-Hou. In

vitro degradation of MAO/PLA coating on Mg-1.21 Li-1.12 Ca-1.0 Y alloy [J]. Frontiers of Materials Science, 2014, 8: 343-353.

[17] HAMDY A S, FARAHAT M. Chrome-free zirconia-based protective coatings for magnesium alloys [J]. Surface and Coatings Technology, 2010, 204: 2834-2840.

[18] ZHOU Wan-qiu, SHAN Da-yong, HAN En-hou, KE Wei. Structure and formation mechanism of phosphate conversion coating on die-cast AZ91D magnesium alloy [J]. Corrosion Science, 2008, 50: 329-337.

[19] ARDELEAN H, FRATEUR I, MARCUS P. Corrosion protection of magnesium alloys by cerium, zirconium and niobium-based conversion coatings [J]. Corrosion Science, 2008, 50: 1907-1918.

[20] ZUO Ke, WANG Xin, LIU Wei, ZHAO Yue. Preparation and characterization of Ce-silane-ZrO 2 composite coatings on 1060 aluminum [J]. Transactions of Nonferrous Metals Society of China, 2014, 24: 1474-1480.

[21] JIANG Qiong, MIAO Qiang, TONG Fei, XU Yi, REN Bei-lei, LIU Zhi-mei, YAO Zheng-jun. Electrochemical corrosion behavior of arc sprayed Al–Zn–Si–RE coatings on mild steel in 3.5% NaCl solution [J]. Transactions of Nonferrous Metals Society of China, 2014, 24: 2713-2722.

[22] LIN C S, LIN H C, LIN K M, LAI W C. Formation and properties of stannate conversion coatings on AZ61 magnesium alloys [J]. Corrosion Science, 2006, 48: 93-109.

[23] ZENG Rong-Chang, LIU Li-Jun, PANG Ting-Ting, ZHANG Fen, ZHANG Wei-Wei, LI Shuo-Qi, CUI Hong-Zhi, HAN En-Hou. Corrosion resistance of silane-modified hydroxide zinc carbonate film on AZ31 magnesium alloy [J]. Acta Metallurgica Sinica (English Letters), 2015, 28: 373-380.

[24] ZENG Rongchang, CHEN Jun, KUANG Jun, ZHANG Jin, WANG Ying. Influence of silane on corrosion resistance of magnesium alloy AZ31 with thermally sprayed aluminum coatings [J]. Rare Metals, 2010, 29: 193-197.

[25] LIU Jian-rui, GUO Yi-na, HUANG Wei-dong. Study on the corrosion resistance of phytic acid conversion coating for magnesium alloys [J]. Surface and Coatings Technology, 2006, 201: 1536-1541.

[26] GUPTA RK, MENSAH-DARKWA K, SANKAR J, KUMAR D. Enhanced corrosion resistance of phytic acid coated magnesium by stearic acid treatment [J]. Transactions of Nonferrous Metals Society of China, 2013, 23: 1237-1244.

[27] CHIU K Y, WONG M H, CHENG F T, MAN H C. Characterization and corrosion studies of fluoride conversion coating on degradable Mg implants [J]. Surface and Coatings Technology, 2007, 202: 590-598.

[28] ZENG Rong-Chang, LIU Zhen-Guo, ZHANG Fen, LI Shuo-Qi, CUI Hong-Zhi, HAN En-Hou.

Corrosion of molybdate intercalated hydrotalcite coating on AZ31 Mg alloy [J]. Journal of Materials Chemistry A, 2014, 2: 13049-13057.

[29] ZHANG Fen, LIU Zhen-Guo, ZENG Rong-Chang, LI Shuo-Qi, CUI Hong-Zhi, SONG Liang, HAN En-Hou. Corrosion resistance of Mg–Al-LDH coating on magnesium alloy AZ31 [J]. Surface and Coatings Technology, 2014, 258: 1152-1158.

[30] MONTEMOR M F, SIMOES A M, CARMEZIM M J. Characterization of rare-earth conversion films formed on the AZ31 magnesium alloy and its relation with corrosion protection [J]. Applied Surface Science, 2007, 253: 6922-6931.

[31] LI Ling-jie, LEI Jing-lei, YU Sheng-hai, TIAN Yu-jing, JIANG Qi-quan, PAN Fu-sheng. Formation and characterization of cerium conversion coatings on magnesium alloy [J]. Journal of rare earths, 2008, 26: 383-387.

[32] RUDD A L, BRESLIN C B, MANSFELD F. The corrosion protection afforded by rare earth conversion coatings applied to magnesium [J]. Corrosion Science, 2000, 42: 275-288.

[33] CAI Jing-shun, CAO Fa-he, CHANG Lin-rong, ZHENG Jun-jun, ZHANG Jian-qing, CAO Chu-nan. The preparation and corrosion behaviors of MAO coating on AZ91D with rare earth conversion precursor film [J]. Applied Surface Science, 2011, 257: 3804-3811.

[34] SONG Ying-wei, SHAN Da-yong, CHEN Rong-shi, ZHANG Fan, HAN En-hou. Formation mechanism of phosphate conversion film on Mg–8.8 Li alloy [J]. Corrosion Science, 2009, 51: 62-69.

[35] ZENG Rong-chang, LAN Zi-dong, CHEN Jun, MO Xian-hua, HAN En-hou. Progress of chemical conversion coatings on magnesium alloys [J]. The Chinese Journal of Nonferrous Metals, 2009, 19: 397-404. (in Chinese)

[36] NIU L Y, JIANG Z H, LI G Y, GU C D, LIAN J S. A study and application of zinc phosphate coating on AZ91D magnesium alloy [J]. Surface and Coatings Technology, 2006, 200: 3021-3026.

[37] NGUYEN V P, MOON S, CHANG D Y, LEE K H. Effect of microstructure on the zinc phosphate conversion coatings on magnesium alloy AZ91 [J]. Applied Surface Science, 2013, 264: 70-78.

[38] NGUYEN V P, LEE K H, CHANG D Y, MOON S. Effects of Zn^{2+} concentration and pH on the zinc phosphate conversion coatings on AZ31 magnesium alloy [J]. Corrosion Science, 2013, 74: 314-322.

[39] NGUYEN V P, LEE K H, CHANG D Y, KIM M, LEE S, MOON S. Zinc phosphate conversion coatings on magnesium alloys: A review [J]. Metals and Materials International, 2013, 19: 273-281.

[40] CHEN Xiao-bo, ZHOU Xian, ABBOTT T B, M A EASTON, BIRBILIS N. Double-layered manganese phosphate conversion coating on magnesium alloy AZ91D: Insights into coating formation,

growth and corrosion resistance [J]. Surface and Coatings Technology, 2013, 217: 147-155.

[41] CUI Xue-jun, LIU Chun-hai, YANG Rui-song, FU Qing-shan, LIN Xiu-zhou, GONG Min. Duplex-layered manganese phosphate conversion coating on AZ31 Mg alloy and its initial formation mechanism [J]. Corrosion Science, 2013, 76: 474-485.

[42] LIU Feng, SHAN Da-yong, HAN En-hou, LIU Chang-sheng. Barium phosphate conversion coating on die-cast AZ91D magnesium alloy [J]. Transactions of Nonferrous Metals Society of China, 2008, 18: s344-s348.

[43] TAKAHIRO I, YOSHITAKE M, KATSUYA T. Composite film formed on magnesium alloy AZ31 by chemical conversion from molybdate/phosphate/fluorinate aqueous solution toward corrosion protection [J]. Surface and Coatings Technology, 2013, 217: 76-83.

[44] ZHANG Chun-Yan, ZENG Rong-Chang, CHEN Rong-Shi, LIU Cheng-Long, GAO Jia-Cheng. Preparation of calcium phosphate coatings on Mg-1.0 Ca alloy [J]. Transactions of Nonferrous Metals Society of China, 2010, 20: s655-s659.

[45] HELLER D K, FAHRENHOLTZ W G, O'KEEFE M J. The effect of post-treatment time and temperature on cerium-based conversion coatings on Al 2024-T3 [J]. Corrosion Science, 2010, 52: 360-368.

[46] WU Guo-song, IBRAHIM J M, CHU P K. Surface design of biodegradable magnesium alloys-a review [J]. Surface and Coatings Technology, 2013, 233: 2-12.

[47] LI Qing, XU Shu-qiang, HU Jun-ying, ZHANG Shi-yan, ZHONG Xian-kang, YANG Xiao-kui. The effects to the structure and electrochemical behavior of zinc phosphate conversion coatings with ethanolamine on magnesium alloy AZ91D [J]. Electrochimica Acta, 2010, 55: 887-894.

[48] ZENG Rong-chang, LAN Zi-dong. Influence of bath temperature of conversion treatment process on corrosion resistance of zinc calcium phosphate conversion film on AZ31 magnesium alloy [J]. The Chinese Journal of Nonferrous Metals, 2010, 20: 1461-1466.

[49] ZENG Rong-chang, LAN Zi-dong, KONG Linghong, HUANG Yuan-ding, CUI Hong-zhi. Characterization of calcium-modified zinc phosphate conversion coatings and their influences on corrosion resistance of AZ31 alloy [J]. Surface and Coatings Technology, 2011, 205: 3347-3355.

[50] ZENG Rong-chang, ZHANG Fen, LAN Zi-dong, CUI Hong-zhi, HAN En-hou. Corrosion resistance of calcium-modified zinc phosphate conversion coatings on magnesium-aluminium alloys [J]. Corrosion Science, 2014, 88: 452-459.

[51] HUSSEIN A M, GARDNER P J, MCARA I W. The standard enthalpies of formation of some zinc

orthophosphate polymorphs [J]. Thermochimica Acta, 1992, 196: 117-123.

[52] ZENG Rong-chang, SUN Xin-xin, SONG Ying-wei, ZHANG Fen, LI Shuo-qi, CUI Hong-zhi, HAN En-hou. Influence of solution temperature on corrosion resistance of Zn-Ca phosphate conversion coating on biomedical Mg-Li-Ca alloys [J]. Transactions of Nonferrous Metals Society of China, 2013, 23: 3293-3299.

[53] XU Luo-min, WANG Xi, LI Lei, KE Zuo. Densification process of cerium-based conversion coatings on AZ31 magnesium alloy [J]. The Chinese Journal of Nonferrous Metals, 2013, 23: 3135-3140.

[54] ZHANG Mi-lin. Cerium chemical conversion coating on a novel Mg-Li alloy [J]. Journal of Wuhan University of Technology-Material Sciience Ed., 2010, 25: 112-117.

[55] ZENG Rong-chang, ZHANG Jin, HUANG Wei-jiu, DIETZEL W, KAINER K U, BLAWERT C, KE Wei. Review of studies on corrosion of magnesium alloys [J]. Transactions of Nonferrous Metals Society of China, 2006, 16: s763-s771.

镁合金 AZ31 表面铈掺杂锌钙磷酸盐化学转化膜腐蚀性能

曾荣昌[1,2]，胡艳[1,2]，张芬[1,2]，黄原定[4]，王振林[3]，李硕琦[1,2]，韩恩厚[5]

1. 山东科技大学 材料科学与工程学院，青岛 266590；

2. 山东科技大学 山东省矿山灾害预防控制重点实验室—省部共建国家重点实验室培育基地，青岛 266590

3. 重庆理工大学 材料科学与工程学院，重庆 400054；

4. MagIC-Magnesium Innovation Center, Helmholtz-Zentrum Geesthacht, Zentrum für Material-und Küstenforschung GmbH, Geesthacht D-21502, Germany ；

5. 中国科学院 金属研究所 国家金属腐蚀控制工程技术研究中心，沈阳 110016

摘要： 在镁合金 AZ31 表面制备了锌钙磷酸盐(Zn-Ca-P)涂层和铈掺杂锌钙磷酸盐(Zn-Ca-Ce-P)涂层。采用电子能谱（EDS）、光电子能谱仪（XPS）、X 射线衍射（XRD）、电子探针（EPMA）和扫描电镜（SEM）以及析氢实验和电化学测试技术研究了涂层的化学成分、形貌和腐蚀性能。结果表明，

两种膜层主要是磷酸盐($Zn_3(PO_4)_2·4H_2O$)，$Mg_3(PO_4)_2$，$Ca_3(PO_4)_2$ 晶体簇和少量的 MgF_2 和 CaF_2 非晶颗粒组成。$CePO_4$ 的形成使 Zn-Ca-Ce-P 膜层更加致密，并具有更好的耐蚀性。两种涂层只能在浸泡前期为 AZ31 基体提供保护作用，随着浸泡时间延长，涂层与基体界面之间电偶腐蚀的发生加快了腐蚀速率。Ce 的存在促进了 Ca 的均匀分布和磷化膜的形成。因此，Zn-Ca-Ce-P 涂层具有作为镁合金底涂层的应用前景。

关键词：镁合金；铈；钙；化学转化膜；腐蚀